Surface Science and Technology

ORIGINAL ARTICLE

Open Access

Corrosion and isothermal interdiffusion properties of Ni–Al coatings under simulated biomass combustion conditions

Yi Xu[1], Zhenhua Wu[1], Hongyu Hu[1], Yuefei Wang[1] and Duoli Wu[1*]

Abstract

The main issue with using biomass fuels in power plants is fireside corrosion. Applying corrosion-resistant coatings is one potential choice. The current study examines how a Ni–Al diffusion coating on austenitic stainless steel reacts to corrosion and interdiffusion (TP347H). Nickel was electrolytically deposited to create Ni–Al coatings, which were then pack aluminized at 650 °C. With an internal layer of Ni and a Ni_2Al_3 outer layer, a homogenous and dense Ni–Al coating was created. Samples were heated to 560 °C for 168 h in an environment designed to simulate the combustion of biomass. A localized corrosion attack was the result. By using isothermal heat treatment in static air at 650 °C or 700 °C for up to 3000 h, interdiffusion was examined. In the course of the interdiffusion process, the Ni_2Al_3 eventually changed into NiAl and Ni_3Al. At both temperatures, porosity formed at the intersection of the Ni–Al coating and the Ni layer and grew with time.

Keywords Ni–Al coatings, Isothermal interdiffusion, High temperature corrosion, Biomass-combustion

1 Introduction

The globe is paying more attention to challenges related to global warming. The utilization of CO_2-neutral fuels, such as biomass, has become more popular recently because CO_2 is one of the leading greenhouse gases. However, problems arise when using biomass as fuel in power plants. Fireside corrosion is one of the critical problems. It is caused by corrosive substances containing sulphur dioxide, hydrogen chloride, and potassium chloride generated by biomass combustion. Fireside corrosion can lead to the premature failure of superheater tubes exposed to high temperatures [1]. This limitation sets the maximum outlet steam temperature for biomass-burning power stations at 540 °C, which reduces their efficiency compared to fossil fuel plants [2]. In addition, even at 540 °C, the corrosion rate in a biomass plant is faster than in a coal-fired plant, leading to components having to be replaced already after 5–10 years. Unlike fossil fuels, corrosion cannot be prevented by employing materials with a greater Cr content. While burning biomass, chromia does not provide protection against the corrosive species present in the flue gas [3]. Applying corrosion-resistant coatings containing elements other than Cr is one option.

Much work has been done on the selection of coating materials for boiler superheaters. Kiamehr [4] tested the reactivity of different oxides with KCl under simulated high temperature corrosion conditions of biomass. The results of the study showed that a significant reaction between KCl and Cr_2O_3 took place after 15 h at 650 °C, but no considerable reaction between KCl and Al_2O_3 was observed. Jonsson [5] found that pure nickel and electroplated nickel also showed good corrosion resistance in KCl under laboratory-simulated corrosion conditions, and no significant reaction between KCl and NiO was observed. Therefore, the preparation of nickel-aluminide

*Correspondence:
Duoli Wu
dlwu@yzu.edu.cn
[1] College of Mechanical Engineering, Yangzhou University, Yangzhou 225127, China

coatings that can form an Al_2O_3 oxide film is a potential optimized option for solving the problem of high-temperature corrosion of biomass.

Aluminide diffusion coatings are deposited using the economical and popular pack aluminizing coating technique. Aluminizing is typically carried out at temperatures higher than 700 °C, which can have negative influences on a steel substrate. A limited amount of work has been published on aluminizing at lower temperatures: Schütze and Rohr aluminized P91 at 650 °C, although the coatings were irregular in thickness, and pores and cracks formed during the coating process [6]. The coating quality was significantly improved in their following work [7]. Wang et al. prepared a coating with an inner layer of FeAl and a thin outer layer of Fe_2Al_5 at 700 °C. The coating was uniform, and no cracks were formed [8]. Xiang et al. deposited Fe-aluminide coatings on P92 steel at 650 °C and investigated the long-run oxidation performance in both steam and air at 650 °C. The findings suggested that under steam and air conditions at 650 °C, the coating would increase the steel's long-term oxidation resistance [9].

The coating lifetime is determined by the depletion of aluminium via two primary mechanisms: I) surface corrosion and II) interdiffusion due to chemical differences between the steel substrate and the coating. The present study considers both degradation mechanisms of a Ni–Al coating deposited onto TP347H via nickel electrolytic deposition, then low-temperature pack aluminizing.

The interdiffusion behaviour of Ni–Al coatings has been extensively studied, but most of the literature refers to higher temperatures than those relevant for biomass combustion, see, e.g. [10], and lower temperatures (between 600 °C and 700 °C) have been studied very seldom. In the temperature range of 655–1000 °C, Janssen and Rieck investigated the layer growth kinetics in Ni–Al diffusion couples but tested for up to only 300 h [11]. Xiang et al. examined the growth kinetics of intermetallic phases in Ni–Al coatings caused by interdiffusion, but in an argon environment and only at 650 °C [12]. Corrosion properties of the aluminized coatings have been well established and have been reported extensively in literature in a variety of chemical environments. Therefore, in order to anticipate the service life of coated components, it is necessary to better understand the interdiffusion performance of Ni–Al coatings at temperatures relative to biomass combustion power plants, in addition to the precise corrosion mechanism. The work also serves as a baseline for understanding the degradation mechanisms for similar coating solutions that have been inserted into full service on superheater tubes in power plants.

2 Experimental procedures

2.1 Sample preparation

The base metal to be coated was TP347H austenitic stainless steel. Table 1 provides the nominal composition of the steel. A TP347H tube with measurements of 32 mm on the outside, 19 mm on the interior, and 10 mm on the thickness was cut into tube pieces using a precision metal cutter. All of the samples were cleaned with ethanol and ground using 1000-grit SiC paper. The samples in the form of rings each had two holes drilled perpendicular to the cross-section. A screw was placed into each hole, and wires were connected to the screws to allow handling during the nickel electroplating process.

2.2 Coating

On TP347H stainless steel, the Ni–Al coating was produced using a two-step procedure. The steel was first electroplated with nickel, and after that, aluminium was added via pack aluminizing. The samples were cleaned using several pre-treatment methods before being nickel electroplated. The samples were washed for three minutes with an anodic degreaser, then rinsed with detergent (soap) and ethanol after three minutes of chemical activation in dry acid. Prior to the final nickel plating, a pre-plating treatment was completed in a Woods nickel [13] striking bath for 5 min, and the current density was 6 A/dm^2. The final nickel-plating procedure was placed in a Watts nickel-plating bath [14]. 100 min of plating at 45 °C and 6 A/dm^2 of current density were used. After an ethanol rinse, the samples were ready for pack aluminization.

Pack aluminizing was performed in a horizontal tube furnace. Pack powders for aluminizing were composed of 82 wt.% Al_2O_3 powder (particle size of 63–200 µm) as an inert filler, 8 wt.% $AlCl_3$ (anhydrous) as an activator, and 10 wt.% Al powder (99.9% purity, maximum particle size of 60 µm) as the aluminium source.

The powders were thoroughly mixed and filled into a cylindrical alumina crucible (outer diameter: 35 mm, inner diameter: 30 mm, length: 50 mm) with the samples embedded in the pack. The crucible was covered with a steel cap, fixed with steel wire and sealed with ceramic cement (produced by Linde AG). After that, the crucible

Table 1 The weight percent of TP347H's nominal chemical composition

Cr	Ni	Mn	C	Si	Nb + Ta	Fe
18	12	2	0.07	< 0.75	< 1.2	Bal

was put inside the argon-flowing tube furnace. At a rate of 18 °C/min, the furnace was heated to 650 °C, and this temperature was maintained for 6 h. The argon gas flow was held after the furnace was shut off while the samples were allowed to cool down to room temperature progressively. The Ni–Al coated samples were taken from the powders after the pack aluminizing, cleaned, and cut into six identical pieces with a precision metal cutter. Following cutting, the samples with Ni–Al coating were ultrasonically degreased in acetone and then dried with ethanol.

2.3 Corrosion exposure

Acetone and ethanol were utilized to clean the tube sections in an ultrasonic bath before depositing KCl. The concave surface of the curved tube sections was coated with a layer of pure KCl (Sigma, 99%). KCl particles were mixed with 2-propanol, and it was then applied to the coating surface. Therefore, a uniform KCl layer that was about 1 mm thick was left behind when the solvent evaporated. The KCl-coated samples were heated to high temperatures in a corrosion test setup that consists of a horizontal electric furnace, a gas mixing panel, and a flue gas cleaning system.

Mass flow controllers were employed to modify the concentration of the several gases that make up the simulated flue gas. The flue gas composition after the burning of straw as determined at a biomass power plant was used to model the gas composition (dry base N_2 82 vol.%, O_2 6 vol.%, CO_2 12 vol.%, SO_2 ppmv, HCl 400 ppmv; the dry gas was lead via a heated humidifier resulting in a final H_2O content of 13.4 vol.%) [15, 16]. Since the typical concentration in straw combustion is around 70 ppm, the HCl concentration utilized here indicates the worst-case scenario. In the corrosion test setup, the samples coated with KCl were heated to 560 °C for 168 h.

2.4 Isothermal heat treatment

The samples with the Ni–Al coating were put in a muffle furnace. The samples were then isothermally heated at 650 °C or 700 °C for 250, 500, 1000, 1500, 2000, 2500, or 3000 h in static laboratory air. Samples were cleaned with ethanol and mounted in epoxy resin following the interdiffusion test. The samples were then ground and polished, with a final polishing step utilizing a Struers Rotopol 22 and 1 µm diamond suspension.

2.5 Characterization of samples

A Scanning Electron Microscope (SEM, Model Quanta 200 ESEM FEG, FEI) fitted with an Energy Dispersive X-ray Spectroscopy (EDS, Oxford Instruments 80 mm^2 X-Max) detector was used to analyze the microstructure and composition of the sample. In the Back-Scattered Electron (BSE) mode, images were acquired. The samples were sputter-coated with a thin carbon coating prior to SEM analysis. Using Image-Pro Plus software, the thickness of several intermetallic phases of Ni–Al layers was measured. The measurements were performed by creating trace features along the phase boundaries, and the software then calculated an average for the distance between trace features.

3 Results and discussion

3.1 Microstructure of Ni–Al coating

Figure 1 displays a cross-sectional image of the coating and the distribution of the main constituents following nickel electroplating and aluminizing. The steel has a double-layered Ni–Al coating that was adhered to it. An exterior Ni_2Al_3 layer (70 µm) and an inner Ni layer (100 µm) made up the double-layer coating. The double-layer structure was consistent with previous results from the literature [9, 14]. By using XRD results and the composition profile of chemical components over the coated surface, the Ni_2Al_3 layer was detected (Fig. 2).

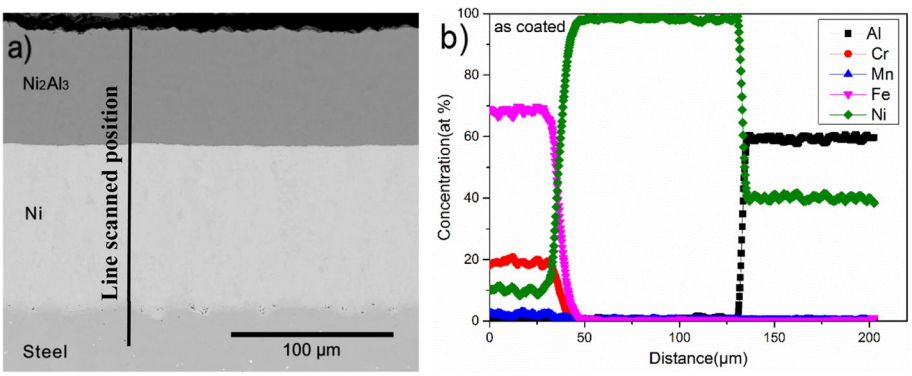

Fig. 1 BSE-SEM micrograph of the Ni–Al coating (**a**) and cross-sectional compositions (**b**)

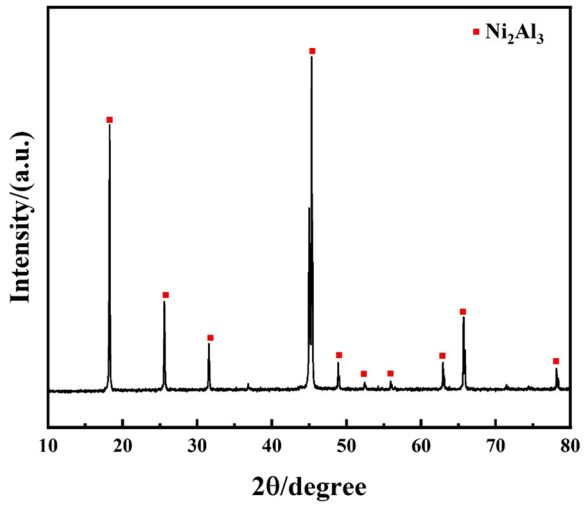

Fig. 2 XRD analysis of the as-received Ni–Al coating

Any stable phase in the Al-Ni binary phase diagram that is stable at 650 °C can develop during the coating preparation process, according to thermodynamics. In reality, kinetics is quite essential. Therefore, only Ni_2Al_3 was discovered right after the coating because Ni_2Al_3's interdiffusion coefficient is significantly greater than that of the other nickel aluminides by at least two orders of magnitude [17].

3.2 Corrosion exposure

Figure 3 illustrates how the exposure caused localized corrosion on the coated surface. At some locations, protective behaviour was observed. In contrast, at the attacked sites, aluminium was selectively removed, presumably as volatile aluminium chloride, leaving behind a porous nickel-enriched area, and a thick layer of corrosion product was present on the coated surface. The voluminous corrosion product, visible as dark grey in the BSE micrographs in Fig. 3, was enriched in Al, K and O with trace levels of Cl and S, as indicated in the EDS elemental maps in Fig. 4. This indicates potassium-aluminate as the outer corrosion product. The BSE contrast of the nickel enriched area indicates the aluminium depletion has caused the formation of NiAl, which is also the first phase expected to form from the phase diagram when Ni_2Al_3 is depleted in aluminium.

Interdiffusion has produced various intermetallic Ni–Al phases as well as apparent porosity at the interface where the nickel layer and the outer coating with enriched aluminum meet.

A porous region, which is visible as a dark line between the nickel layer and the aluminium-enriched outer part, presumably originates from the Kirkendall effect due to differences in diffusion fluxes of aluminium and nickel across the interface. In several locations, this led to the de-scaling of the aluminium-rich outer part of the coating. The de-scaling probably happened either during cooling after testing or during sample preparation.

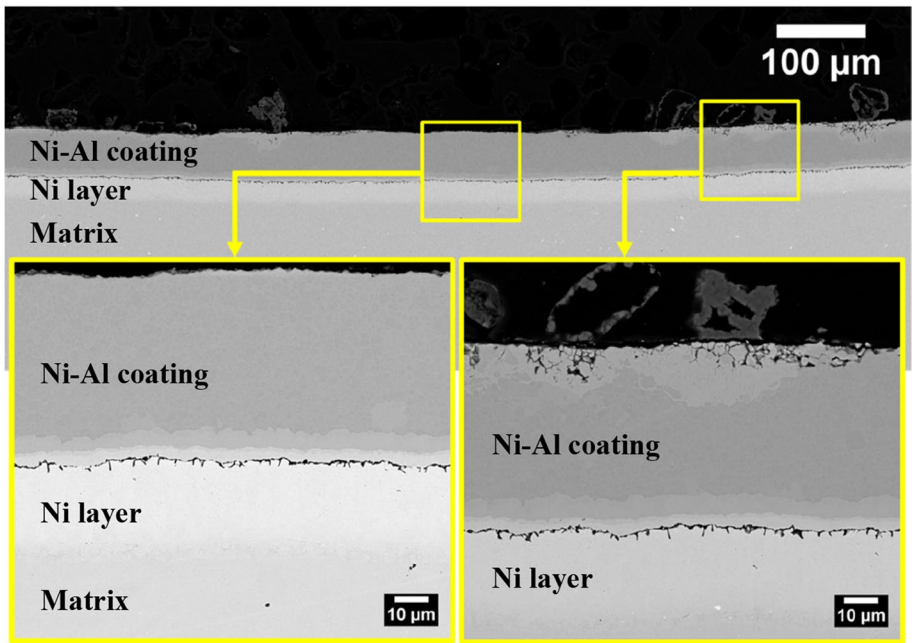

Fig. 3 BSE-SEM micrographs of the exposed Ni–Al coating

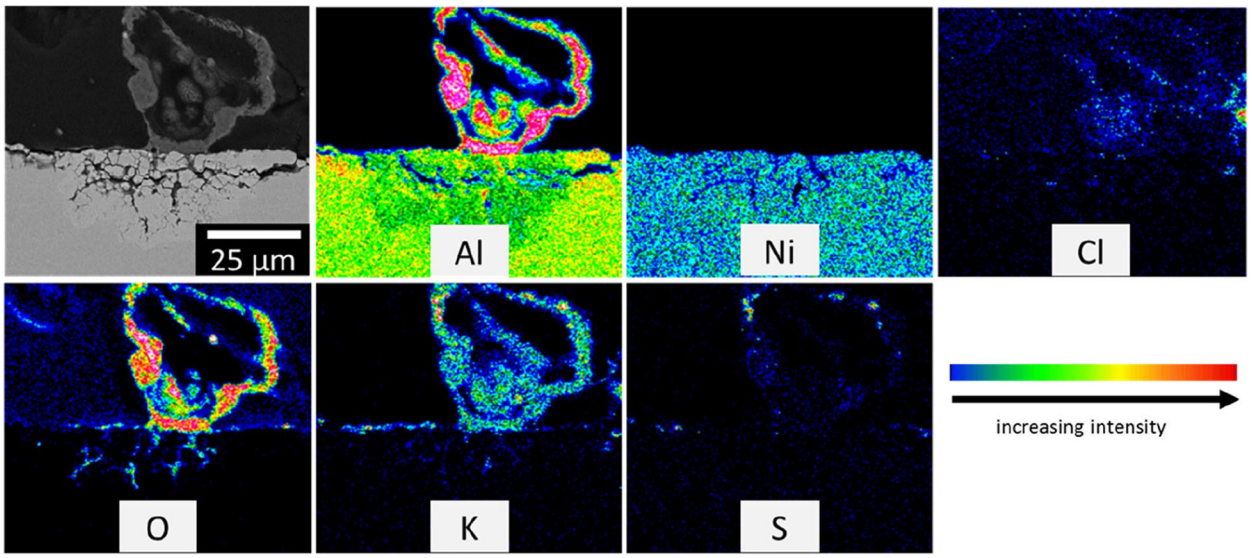

Fig. 4 BSE-SEM micrograph and EDS elemental maps showing the chemical composition across the exposed Ni–Al coating

3.3 Isothermal heat treatment at 650 ℃

After being subjected to isothermal heat treatment at 650 °C for 500, 1500, and 3000 h, the Ni–Al coatings are shown in a cross section in Fig. 5. Besides the initial Ni_2Al_3 phase layer, NiAl, Ni_5Al_3 and Ni_3Al layers formed. The NiAl appeared as two "layers" in BSE contrast with a thick NiAl layer and a thin Al-rich NiAl layer were found, which is in line with the findings of other authors [15, 18].

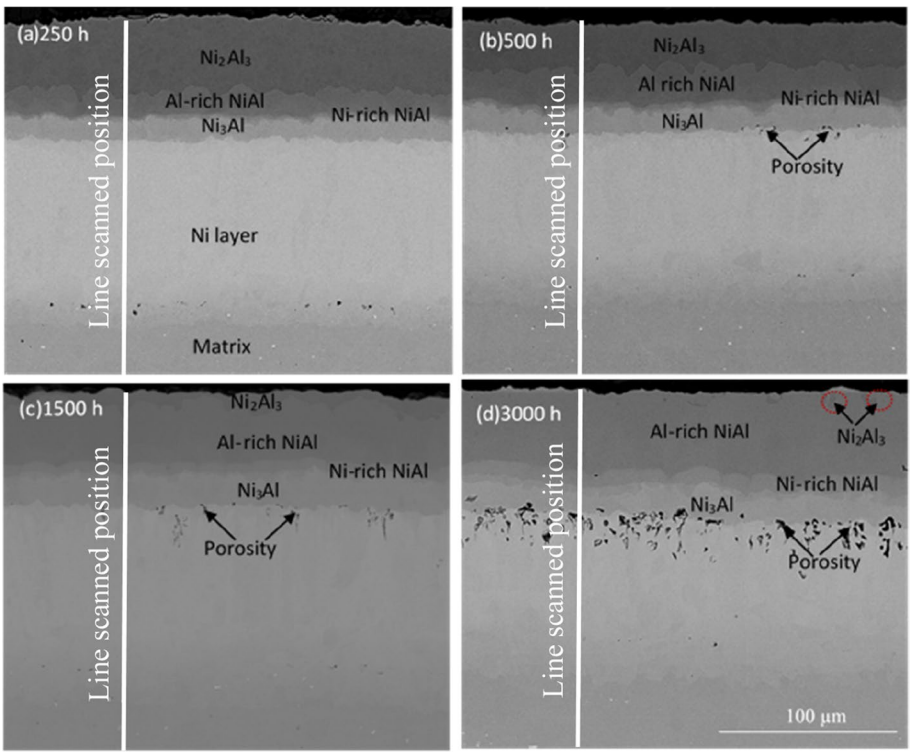

Fig. 5 BSE micrographs of the Ni–Al coating after being subjected to isothermal heat treatment at 650 °C for 250 h (**a**), 500 h (**b**), 1500 h (**c**), and 3000 h (**d**), respectively

As shown in Fig. 5(a), the outer Ni_2Al_3 phase transformed into an Al-rich NiAl phase, which was due to the similarity of their structures. Ni_2Al_3 and Al-rich NiAl phases were based on the same structure. Both of them were derived from bcc structure with a slight difference in the Ni vacancies distribution [19]. The Ni vacancies were randomly distributed in the Al-rich NiAl phase, while they were ordered in sheets perpendicular to the cube diagonal in the Ni_2Al_3 phase [20]. Ni_5Al_3 was not observed at the NiAl/Ni_3Al interface, even though this could be expected from the phase diagram. Jiang et al. suggested that the formation of Ni_5Al_3 was difficult at the NiAl/Ni_3Al interface, which agreed well with the findings of Xiang et al. [21]. Their research demonstrated that the growth of the Ni_5Al_3 phase layer began only after the Ni_2Al_3 phase had entirely been consumed [14].

These intermetallic layers grew as a function of time at the expense of the outermost Ni_2Al_3 layer, and porosities started to appear at the interface of Ni–Al / nickel layer, see Fig. 5(b). These are likely Kirkendall voids that developed as a result of variations in the inherent diffusivities of nickel and aluminium. The porous region expanded gradually with time. Nickel leaves the nickel layer much more quickly during the interdiffusion process compared to how quickly aluminium diffuses into nickel [13, 18].

After 1500 h, only a thin layer of Ni_2Al_3 was left at the surface. After 3000 h, the Ni_2Al_3 phase had been almost entirely converted, and the surface of the sample included the Al-rich NiAl phase, see Fig. 5(c).

After the interdiffusion test at 650 °C for 3000 h, the coating samples experienced only slight oxidation and a reasonably thin oxidation film formed on the surface. During the whole process, a significant reduction in Al was not apparent at the surface.

According to the composition profiles shown in Fig. 6, the Ni layer acted as a barrier, which prevented aluminum from diffusing into the substrate from the coating. When examining the penetration depth on the profiles for different diffusion times, it is evident that the diffusion of Al into the Ni layer from the Ni–Al coating occurred at a somewhat modest rate. The total penetration depth of Al after 3000 h was around 15–20 μm.

Cr and Fe are also diffused into the Ni layer at the point where it meets the steel substrate. For around 30 μm, Cr and Fe entered the Ni layer. However, these two elements did not encounter Al from the outer coating before 3000 h had elapsed.

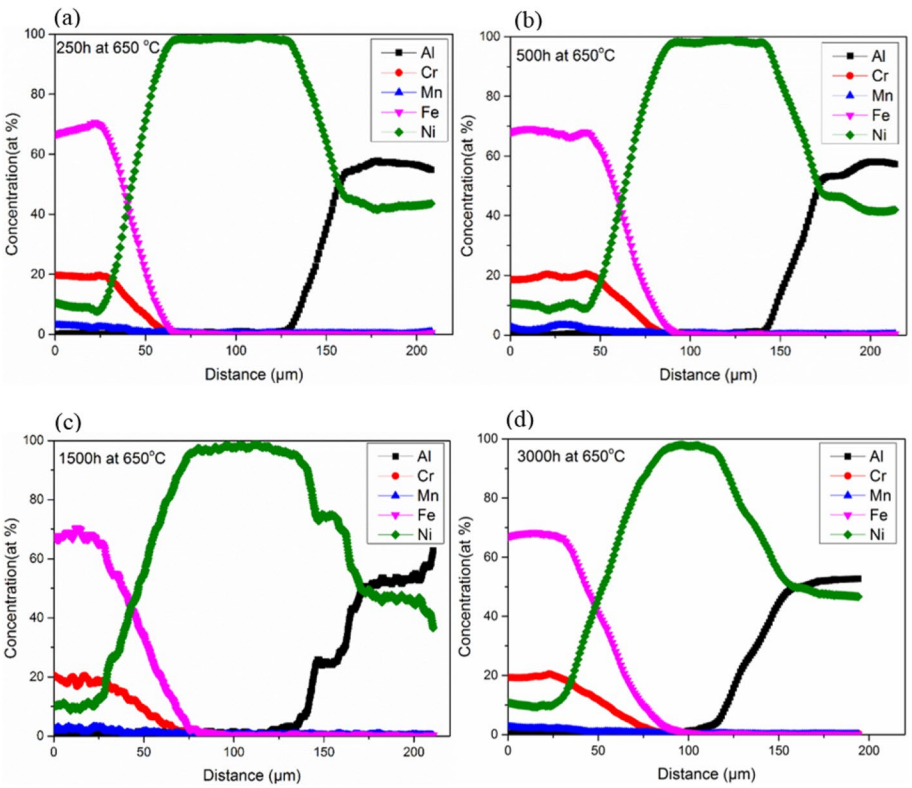

Fig. 6 Composition profiles of the Ni–Al coating after being subjected to isothermal heat treatment at 650 °C for 250 h (**a**), 500 h (**b**), 1500 h (**c**), and 3000 h (**d**), respectively

3.4 Isothermal heat treatment at 700 ℃

In order to test the coating under a more accelerated condition, the interdiffusion experiment was then performed at 700 °C. The cross-sectional images of the Ni–Al coatings after isothermal heat treatment at 700 °C for 500 h, 1500 h and 3000 h are shown in Fig. 7. Compared with the coating morphology at 650 °C in Fig. 5, the interdiffusion took place much more rapidly at 700 °C.

After 250 h, the Ni–Al coating mainly consisted of Al-rich NiAl, Ni-rich NiAl and Ni_3Al, with only local areas of Ni_2Al_3 in the outermost layer. Ni_5Al_3 was not observed at 700 °C, which is also the upper limit for the formation of this phase according to the binary phase diagram. The coating structure after 500 h of interdiffusion is shown in Fig. 7(b). As was observed at 650 °C, porosities also formed at 700 °C. The porosity formation was much more severe compared to the same time at 650 °C. As shown in Fig. 7(d), after 3000 h, the Ni–Al coating was composed of an outer Al-rich NiAl phase layer, an inner Ni_3Al phase layer and the Ni-rich NiAl phase layer in between has started to grow at the expense of both Al-rich NiAl and Ni_3Al. The porosity formation at the interface between the Ni layer and the Ni–Al coating was so severe that it can be envisioned that it will soon lead to coating spallation.

After the interdiffusion tests up to 3000 h, the coating samples experienced only slight oxidation and a reasonably thin oxide film formed on the surface. During the whole process, no significant surface depletion of Al was visible at the outer surface.

At a specific time, the growth of the Al-rich Ni–Al phase stopped, and the Ni-rich Ni–Al phase started to grow faster. This was due to a change in the predominant species in the different intermetallic stages. Al was found to be the dominant diffusing species in Ni_2Al_3 and Al-rich NiAl phases. However, Ni diffusion was predominant for Ni-rich NiAl and Ni_3Al phases. At some stage, the inward diffusion of Al must lead to a decrease in the Al content of the surface layer to a specific value. The formation of an Al-rich NiAl phase will not continue below this value, and the opposite process of Ni-rich NiAl layer growth by outward diffusion of Ni will be initiated [22].

As shown in Fig. 8, at 700 oC the interdiffusion between Ni and Fe/Cr at the nickel/steel interface took place more rapidly. After 3000 h, the total penetration depth of Fe and Cr was about 40 μm. The Cr and Fe elements in the matrix diffused across the Ni layer and began to enter the Ni–Al coating. In principle, the inner Ni layer can be made sufficiently thick to prevent the Al from the coating reaching the steel. In addition, the Ni layer also acts

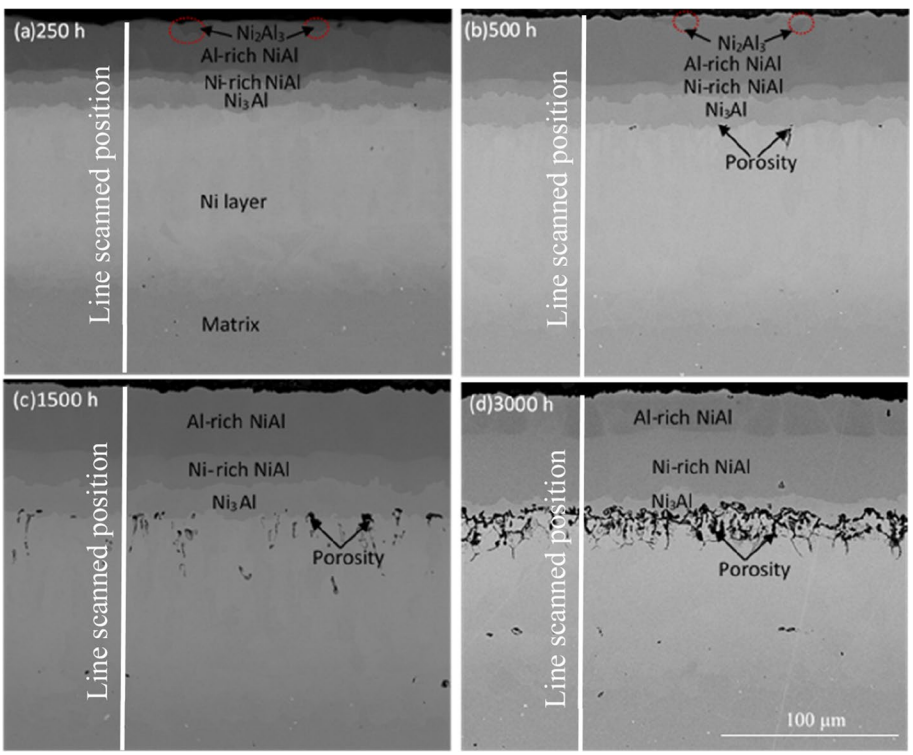

Fig. 7 BSE micrographs of the Ni–Al coating after being subjected to isothermal heat treatment at 700 °C for 250 h (**a**), 500 h (**b**), 1500 h (**c**) and 3000 h (**d**)

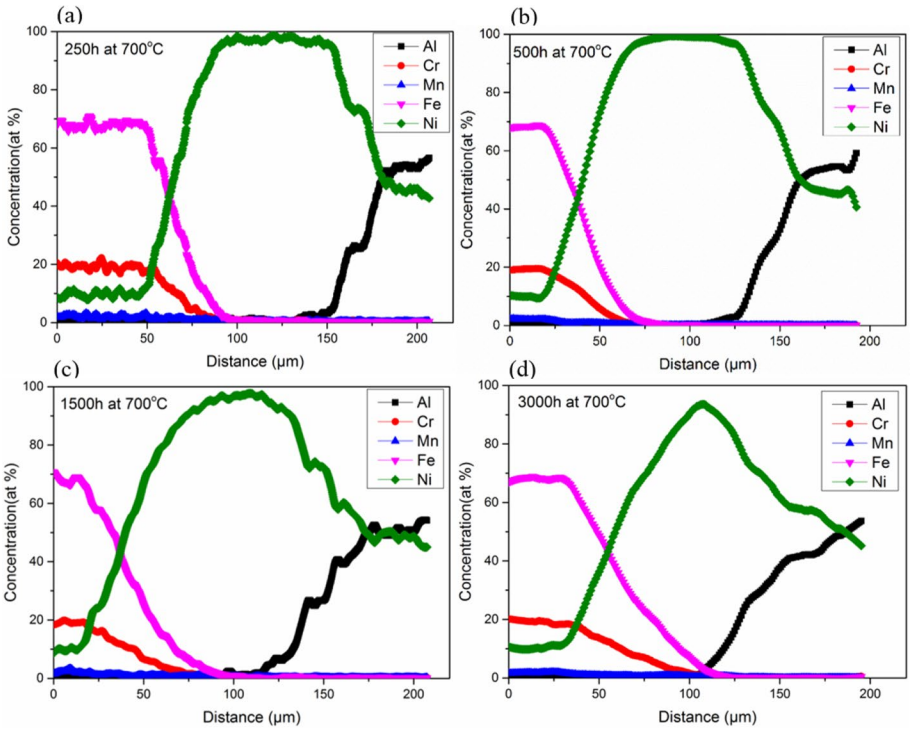

Fig. 8 Composition profiles of the Ni–Al coating after being subjected to isothermal heat treatment at 700 °C for 250 h (**a**), 500 h (**b**), 1500 h (**c**), and 3000 h (**d**), respectively

as a bonding layer, which helps to improve the adhesion between the coating and substrate. However, the Ni layer can also lead to the formation of porosity at the interface of the inner Ni layer and outer coating. It is therefore, the optimal Ni thickness should be evaluated from both aspects.

3.5 Growth kinetics of different intermetallic phases in the coating

The thicknesses of several layers were plotted as a function of the square root of interdiffusion time, as shown in Fig. 9, to investigate the kinetics of intermetallic phase growth in the coating. The sum of the layer thicknesses was also plotted, revealing that there was variation in coating thicknesses on the different samples.

In general, the Ni_2Al_3 was gradually consumed as NiAl (sum of Al rich-NiAl and Ni rich-NiAl) and Ni_3Al were formed. At 650 °C, both Al rich-NiAl and Ni rich-NiAl zones continued to grow and followed a parabolic growth law within the exposure times tested (up to 3000 h). It is to be expected that the thickness of the NiAl zone will start to decrease soon after 3000 h since almost all Ni_2Al_3 has been consumed, and Ni_3Al will start to grow at the expense of NiAl as further Al is lost through the interdiffusion into the nickel.

At 700 °C, the transformation from Ni_2Al_3 into NiAl and Ni_3Al took place much more rapidly than at 650 °C. As shown by the conversion of Al-rich NiAl into Ni-rich NiAl in Fig. 6, the Ni_2Al_3 was already nearly totally converted after 500 h, and the Al depletion of Al rich-NiAl had begun. When 1000 h have passed, the Al rich-NiAl zone's expansion has come to an end, and the Al rich-NiAl phase is starting to deplete in aluminum. However, the Ni rich-NiAl continued to grow even after 3000 h, which was related to a shift of the predominant species in Al rich-NiAl and Ni rich-NiAl.

At both temperatures, the growth of the Ni_3Al phase stops following a parabolic behaviour after 1000–1500 h of testing; it is hypothesized that this is related to the formation of porosities at the interface, limiting the diffusion flux across the interface between Ni and Ni_3Al.

The useful service life of Ni–Al coatings can typically be defined as having ended once the NiAl phase is consumed. The reason for this is that the content and diffusivity of Al in NiAl are still sufficiently high to form a protective oxide scale [23], but when the outer layer has been totally transformed into Ni_3Al, the coating will no longer be protective. As for the Ni_3Al phase, a stable and protective Al_2O_3 scale can only be formed at temperatures above 1200 °C [24]. At lower temperatures, the diffusion of aluminium in Ni_3Al is not sufficiently rapid to

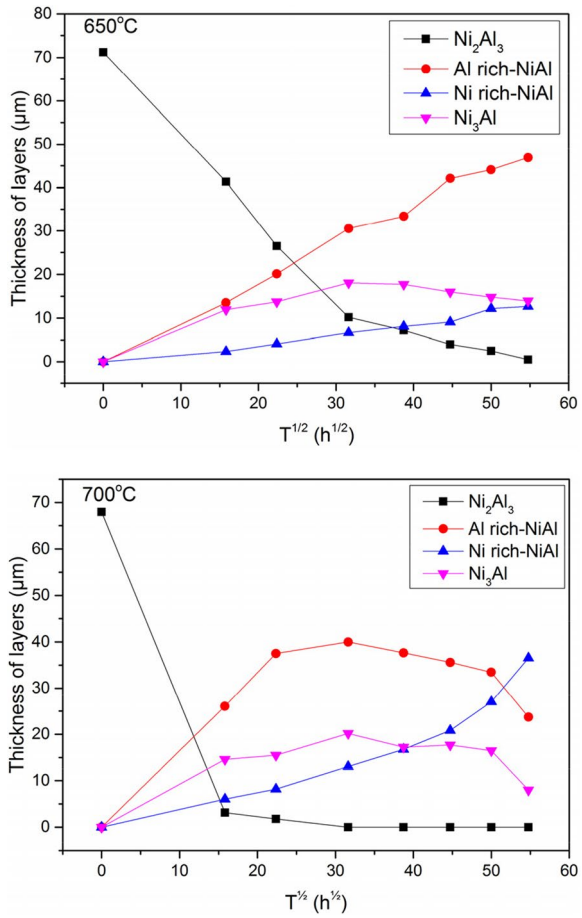

Fig. 9 Growth kinetics of different intermetallic phases in the Ni–Al coating at 650 °C and 700 °C

supply enough Al to stabilise a protective oxide. Furthermore, the oxidation of Ni_3Al was associated with vacancy production, which can lead to the formation of voids and subsequent scale spallation [25].

It is, therefore, essential to track the changes in the NiAl phase, as the oxidation resistance and the service life of the coating are entirely dependent on the presence of a NiAl phase. Our ongoing research aims to develop a lifespan model for the Ni–Al coating by combining the corrosion data and growth dynamics of the NiAl phase during isothermal heat treatment.

3.6 Overall discussion

The corrosion testing for 168 h at 560 oC under conditions simulating biomass combustion revealed localized attack with selective removal of aluminium. The corrosion behaviour was significantly better than the behaviour of uncoated steel TP347 tested under similar conditions. However, spallation of the Ni–Al coating was also observed after corrosion testing, which may prove to be a limiting factor to the application of this type of coating to real superheater tubes, especially in combination with thermal cycling.

The interdiffusion behaviour was analysed at 650 °C and 700 °C. The useful service life of Ni–Al coatings can typically be defined as limited by the consumption of the NiAl phase since the content and diffusivity of Al in NiAl can be expected to be sufficiently high to form a protective oxide scale. At both test temperatures, the NiAl phase continued to be present in the outermost layer after 3000 h had elapsed. In power plants, the actual temperature is below 600 °C, so that the aluminium depletion would be much slower, and the performance of these coatings should be more promising. In the isothermal heat-treated samples, no spallation was observed. With time and at both temperatures, the number of pores at the junction of the Ni–Al coating and the Ni layer increased.

The Ni layer served as a helpful diffusion barrier since it prevented elements from the steel, such as Fe and Cr, from diffusing into the coating, as well as limiting the inward diffusion of aluminium from the coating into the substrate. In light of the coating's service life, it would be preferable to stop Al from penetrating the steel matrix. In this regard, the inner Ni layer's original thickness should be greater than the Al penetration depth into the inner Ni layer. However, the Ni layer itself was detrimental as it diffused rapidly into the Ni–Al coating. At the Ni–Al coating/Ni layer interface, porosity then developed and expanded with time in both cases. This would constitute a limitation for the application of Ni–Al coatings, as peeling may happen in an actual application.

4 Conclusions

Coating resulted in surface layers of Ni_2Al_3 and Ni with a thickness of 70 µm and 100 µm, respectively, from electroplating followed by pack cementation.

Corrosion tests at 560 oC for 168 h in an atmosphere mimicking aggressive biomass combustion resulted in localized attack with selective removal of Al. The Ni–Al had spalled in many places following corrosion tests at 560 °C.

Coated samples were isothermally heat-treated in static air at 650 oC and 700 oC for up to 3000 h. The initial Ni_2Al_3 phase gradually transformed into the NiAl phase and the Ni_3Al phase throughout the interdiffusion process.

Interdiffusion led to the formation of porosity at the interface between the Ni–Al coating and the Ni layer. The porosity region extended over time at 650 °C and 700 °C without causing spallation.

Acknowledgements
This research was funded by the National Natural Science Foundation of China (52101100), the General Project of Natural Science Research in Colleges and Universities of Jiangsu Province (21KJB430008), Yangzhou City-Yangzhou University Cooperation Foundation (YZ2023208) and the Qing Lan Project of Yangzhou University (2022).

Authors' contributions
Yi Xu: Methodology, Experiment, Writing-Review & Editing; Zhenhua Wu: Methodology, Experiment, Writing; Hongyu Hu: Methodology, Experiment, Writing-Review & Editing; Yuefei Wang: Methodology, Experiment, Formal Analysis, Writing-Review & Editing; Duoli Wu: Conceptualization, Writing-Original Draft, Funding.

Availability of data and materials
Not applicable.

Declarations

Ethics approval and consent to participate
Not applicable.

Competing interests
The authors declare that they have no known competing financial interests or personal relationships that could have appeared to influence the work reported in this paper.

Received: 6 September 2023 Revised: 28 October 2023 Accepted: 14 November 2023
Published online: 29 November 2023

References

1. Sadeghimeresht E, Reddy L, Hussain T, Huhtakangas M, Markocsan N, Joshi S (2018) Influence of KCl and HCl on high temperature corrosion of HVAF-sprayed NiCrAlY and NiCrMo coatings. Mater Des 148:17–29
2. Yin CG (2020) Development in biomass preparation for suspension firing towards higher biomass shares and better boiler performance and fuel rangeability. Energy 196:117129
3. Zhang SC, Li HB, Jiang ZH, Zhang BB, Li ZX, Wu JX et al (2020) Chloride- and sulphate-induced hot corrosion mechanism of super austenitic stainless steel S31254 under dry gas environment. Corros Sci 163:108295
4. Kiamehr S, Lomholt TN, Dahl KV, Christiansen TL, Somers MAJ (2016) Application of aluminum diffusion coatings to mitigatethe KCl-induced high-temperature corrosion. Corros Mater 1:82–94
5. Jonsson T, Slomian A, Lomholt TN, Kiamehr S, Dahl KV (2015) Microstructural investigations of pure nickel exposed to KCl induced high temperature corrosion. Mater High Temp 32:44–49
6. Rohr V, Schütze M (2004) Novel low temperature diffusion coatings for heat exchanger materials. Materials Science Forum 461–464:401–408
7. Rohr V, Schütze M, Fortuna E, Tsipas DN, Milewska A, Perez FJ (2005) Development of novel diffusion coatings for 9–12 % Cr ferritic-martensitic steels. Mater Corros 56:874–881
8. Wang YQ, Zhang Y, Wilson DA (2010) Formation of aluminide coatings on ferritic–martensitic steels by a low-temperature pack cementation process. Surf Coat Technol 204:2737–2744
9. Xiang ZD, Rose SR, Datta PK (2006) Long-term oxidation kinetics of aluminide coatings on alloysteels by low temperature pack cementation process. J Mater Sci 41:7353–7360
10. Susan DF, Marder AR (2001) Ni–Al composite coatings: diffusion analysis and coating lifetime estimation. Acta Mater 49:1153–1163
11. Janssen MMP, Rieck GD (1967) Reaction diffusion and Kirkendall-effect in the nickel-aluminum system. Transactions of the Metallurgical Society of AIME 239:1372–1385
12. Xiang ZD, Zeng D, Zhu CY, Wu DJ, Datta PK (2012) A phenomenological model for lifetime design of Ni_2Al_3/Ni hybrid coating formed on creep resistant ferritic steels. J Mater Sci 47:257–266
13. Yazdani S, Mesbah M, Dupont V, Vitry V (2023) Microstructure, wear and crack propagation evolution of electrodeposited nickel-nano diamond composite coatings: molecular dynamic modeling and experimental study. Surf Coat Technol 462:129500
14. Mbugua NS, Kang M, Zhang Y, Ndiithi NJ, Bertrand GV, Yao L (2020) Electrochemical deposition of Ni, NiCo alloy and NiCo–ceramic composite coatings—a critical review. Materials 13:3475
15. Okoro SC, Montgomery M, Frandsen FJ, Pantleon K (2014) High temperature corrosion under laboratory conditions simulating biomass-firing: a comprehensive characterization of corrosion products. Energy Fuels 28:6447–6458
16. Nielsen HP, Frandsen FJ, Dam-Johansen K (1999) Lab-scale investigations of high-temperature corrosion phenomena in straw-fired boilers. Energy Fuels 13:1114–1121
17. Blackford JR, Jones H, Atkinson HV, Tidbury LE, King S (1994) Hot Isostatic Pressing 93. Elsevier Science B.V, Amsterdam, p 301–308
18. Shiomi S, Miyake M, Hirato T, Sato A (2011) Aluminide coatings fabricated on nickel by aluminium electrodeposition from DMSO2-based electrolyte and subsequent annealing. Mater Trans 52:1216–1221
19. Taylor A, Doyle NJ (1972) Further studies on the nickel-aluminium system. I. β-NiAl and δ-Ni_2Al_3 phase fields. J Appl Crystallogr 5:201–209
20. Thevand A, Poize S, Crousier JP, Streiff R (1981) Aluminization of nickel-formation of intermetallic phases and Ni_2Al_3 coatings. J Mater Sci 16:2467–2479
21. Jiang SY, Li SC (2011) Valence electron structure calculation and interface reaction prediction of phases in Ni-Al system. Rare Metal Mat Eng 40:1355–1360
22. Bogdanov A, Kulevich V, Shmorgun V, Taube A (2022) Formation of thermally grown aluminum oxide scale on the surface of Ni_2Al_3/Ni layered coating. Oxid Met 98:199–216
23. Si XQ, Li C, Bo YF, Qi JL, Feng JC, Cao J (2020) The role of Al diffusion behavior in the process of forming a super-reliable Al_2O_3 protective layer during reactive air aluminization. Appl Surf Sci 518:146242
24. Li Q, Long DJ, Song P, Li ZH, Zhang RQ, Chen H et al (2022) Alumina grain growth and grain boundary segregation of FeCrAl-based oxide dispersion-strengthened alloys at high temperature. Corros Sci 208:110630
25. Zhu DD, Wang XL, Zhao J, Lu J, Zhou YC, Cai CY et al (2020) Effect of water vapor on high-temperature oxidation of NiAl alloy. Corros Sci 177:108963

Publisher's Note